

Article

An Electro-Thermal Model for LFP Cells: Calibration Procedure and Validation

Michele Barbieri, Massimo Ceraolo, Giovanni Lutzemberger *  and Claudio Scarpelli

Department of Energy, Systems, Territory and Constructions, University of Pisa, 56126 Pisa, Italy; m.barbieri1@studenti.unipi.it (M.B.); massimo.ceraolo@unipi.it (M.C.); claudio.scarpelli@phd.unipi.it (C.S.)

* Correspondence: giovanni.lutzemberger@unipi.it; Tel.: +39-050-221-7311

Abstract: Lithium batteries for energy storage systems are a prominent solution for both stationary and mobile applications. Electro-thermal modelling of the cell is a useful tool for monitoring voltage and temperature in order to predict battery behaviour especially in cases of critical operative conditions. This paper provides a modelling approach focusing on the calibration of parameters of an electro-thermal model for large prismatic LFP lithium cells. The designed model is tuned by means of experimental tests that identify a set of parameters that are function of a cell's state-of-charge and temperature. The model outputs are voltage, cell surface, and internal temperature profiles, which are validated against experimental data referring to realistic working conditions, even providing an intense level of thermal stress. The model accuracy is marked by a voltage mean average error lower than 1% and a mean cell surface temperature deviation lower than 1 K.

Keywords: lithium; battery; model; experimental; test



Citation: Barbieri, M.; Ceraolo, M.; Lutzemberger, G.; Scarpelli, C. An Electro-Thermal Model for LFP Cells: Calibration Procedure and Validation. *Energies* **2022**, *15*, 2653. <https://doi.org/10.3390/en15072653>

Academic Editor: Holger Hesse

Received: 25 February 2022

Accepted: 2 April 2022

Published: 5 April 2022

Publisher's Note: MDPI stays neutral with regard to jurisdictional claims in published maps and institutional affiliations.



Copyright: © 2022 by the authors. Licensee MDPI, Basel, Switzerland. This article is an open access article distributed under the terms and conditions of the Creative Commons Attribution (CC BY) license (<https://creativecommons.org/licenses/by/4.0/>).

1. Introduction

Lithium batteries are energy storage systems typically considered in stationary applications and electric transportation. Their main features are high energy and power density, low self-discharge rate, extended cycle life, and an even more affordable cost, resulting in them being the benchmark amongst cell battery chemistries [1,2]. However, one of the main limiting factors is represented by some degradation effects caused by battery working conditions outside the ideal range of temperature [3,4].

Electro-thermal modelling of lithium batteries is a viable way of estimating profiles of voltage and temperature under working conditions to determine whether the cell is operating under its ideal specifications.

Many studies reported in the literature deal with the definition of a reliable battery model, able to predict the electrical and thermal behaviour from a single lithium cell to a whole battery pack. Two main different approaches can be distinguished: physics-based models and equivalent electrical circuit (EEC) models. Physics-based models aim to provide full information on the inner electrochemical dynamics of a battery at the cell level, with main application field in chemistry research and by battery manufacturers. Generally, they make use of complex sets of coupled partial differential equations to explain how the cell potential is produced and affected by the electrochemical reactions that take place inside the cell itself. These models are capable of predicting the cell/battery electrical and thermal behaviour over wide ranges of operative working conditions (e.g., high thermal stresses and wide state-of-charge variations) [5–8]. Anyhow, despite the good level of accuracy, they are still difficult to apply in real-time applications because they suffer from a very high level of complexity, due to the kind of equations used, the high level of detail, and very high model orders.

On the other hand, equivalent electrical circuit (EEC) models have gained much interest in real-time applications due to their simplified model structure and their easiness to be identified. EEC models use electrical networks to mimic the main significant battery

behaviours in terms of either electrical and thermal quantities that can be easily measured from the battery outer terminals (such as battery voltage and current, as well as battery case temperature) [8–12]. This approach can be applied both to model the behaviour of a single cell as well as to model a whole battery pack system, without significant complexity arising. From an external point of view, the whole battery system is modelled as a “black box”, containing an electrical network interfacing with the outer systems with one 2-terminal DC electric port, easy to be integrated inside vehicle powertrains. These reasons make this kind of approach the most preferable for battery users and systems assemblers (e.g., EV manufacturers).

In this paper, an EEC-based electro-thermal model for a lithium cell is given, relying on calibration tests and providing a streamlined procedure leading to a precise calculation of model parameters, in function of a wide range of cell state-of-charge (SOC) and temperatures. In this way, the proposed methodology aims to have the advantage of the physics-based model (i.e., of being able to simulate the electro-thermal behaviour of a lithium battery over a wide range of working conditions) and at the same time the advantage of the EEC models—the simplicity of implementation and ease of utilization.

The proposed model was designed starting from the simplified approach already proposed by the authors in [13], implementing additional upgrades: first of all, the model was applied to a large prismatic lithium cell in which electrical dynamics during charge and discharge were simulated through a sophisticated equivalent electrical circuit, and its thermal behaviour was simulated by a lumped parameters two-node equivalent thermal network. In this way, in addition to the estimation of cell surface temperature that can be easily compared with experimental measures, an estimation of internal temperature was also given. This last aspect is typically not available by direct measurement for commercial cells, unless through a significative structural adaptation, due to damage risk [14].

The quality and the robustness of the model results were evaluated by several comparisons between simulations and experimental data. In particular, the model estimation of cell voltage and surface temperature was compared to the experimental recorded values.

The paper structure is here presented: in Section 2, the characteristics of the cell under test are displayed, as well as the experimental equipment adopted for performing all the experimental tests. Section 3 illustrates the proposed electro-thermal model and how it is calibrated via experimental tests. In Section 4, the model is validated against realistic working conditions, including also current profiles that can provide high electrical stress, causing wide temperature variation.

2. Experimental Setup

The lithium cell tested and characterized in this paper is a prismatic LFP cell, the specifications of which are in Table 1. The experimental setup was composed by a Digatron[®] battery cycler [15], and a Binder[®] climatic chamber [16], in which the cell under test was placed. Three K-type probes measuring air temperature were placed in various places of the climatic chamber, far above the cell. For the cell temperature measurement, two ring thermocouples were placed at the cell electrodes, while four probes were located on the cell surface: three on the upper surface, one in the middle of the lowest surface, as in Figure 1. For all thermocouples, tolerance values were ± 1.5 K in a range of validity from 233.15 K to 623.15 K. Reference temperatures for room, electrode, and cell surface were obtained by averaging the values recorded by the respective thermocouples: for example, cell surface temperature was obtained by aggregating measures from the four sensors installed on the plastic case. A direct measure of internal cell temperature was not available because of the practical impossibility of reaching the core without damaging the cell. However, for electro-thermal model characterization purposes only, the internal cell temperature could be approximated by means of the electrode temperature, as in [9].

Table 1. Cell specifications.

Cell Typology	Lithium LFP
Geometry (mm)	Prismatic 114 × 203 × 61
Nominal capacity at 1C rate (Ah)	60
Nominal voltage (V)	3.2
Voltage range (V)	max 4.0–min 2.8
Max temperature (K)	353.15
Max continuous discharge C-rate (A/Ah)	3
Standard charge	0.5C CC-CV at 293.15 K

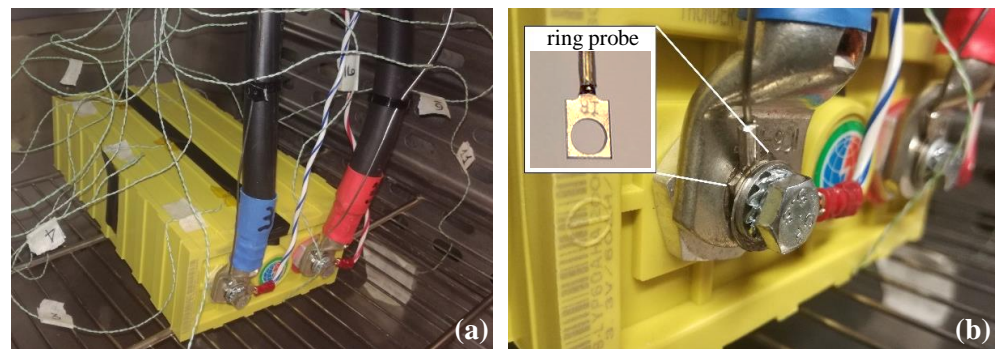


Figure 1. Cell inside the climatic chamber. (a) Any labelled thermocouple refers either to cell surface, electrode, or air temperature. (b) Detail of the ring probe placed at the cell positive electrode.

3. Cell Electro-Thermal Model

3.1. Electric Model and Calibration of Its Parameters

From an electrical point of view, the cell was modelled by an equivalent electrical circuit, a scheme of which is depicted in Figure 2.

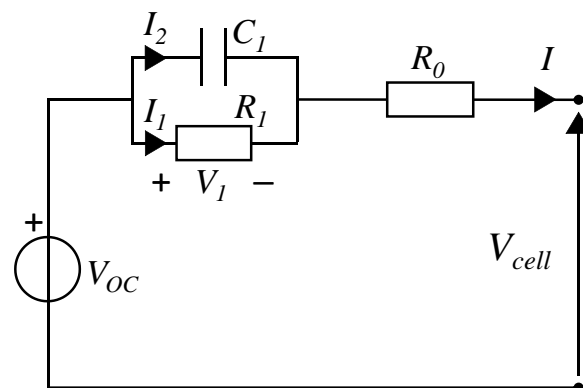


Figure 2. Equivalent electrical circuit for the lithium cell.

This model is often considered in the literature [17], and the authors applied it in other studies [18,19]. The electric network consists of a voltage source indicating the open circuit voltage of the cell (V_{OC}), a parallel R_1C_1 block made by the resistance R_1 and the capacitance C_1 , and an internal ohmic resistance (R_0).

The electrical model dynamic can be completely determined by the following equations, which respectively describes the cell output voltage and the voltage of the R_1C_1 block in function of the cell output current I and the model parameters:

$$V_{cell} = V_{OC} - V_1 - I \cdot R_0 \quad (1)$$

$$\dot{V}_1 = \frac{I}{C_1} - \frac{V_1}{R_1 C_1} \quad (2)$$

$$I = I_1 + I_2 \quad (3)$$

where I_1 and I_2 are the currents which respectively flow on the lower and upper branches of the R_1C_1 block. All the elements in the previous equation are time-variant due to the fact that open circuit voltage, resistances, and the capacitance are a function of both cell temperature and SOC. In the present article, SOC is defined as follows, with C_n being the nominal capacity of the cell acquired from the specifications of Table 1:

$$SOC = 1 - \frac{\int Idt}{C_n} \quad (4)$$

For this electrical model, the parameters to be estimated are V_{OC} , R_0 , R_1 , and C_1 , and the following experimental procedure was used to obtain, for each parameter, a set of discontinuous values corresponding to discrete estimation of both SOC and cell temperature. In order to determine this set of electric parameters of the cell, a series of three multiple step tests was performed on a fully charged battery, setting the climatic chamber temperature at 298.15 K, 313.15 K, and 328.15 K, respectively.

The multiple step test (MST) consisted in 10 intermittent discharging steps, each one followed by a rest phase lasting one hour. After the tenth rest phase, the cell was charged back with 10 other symmetrical charging steps, again followed by an hour-long pause. Every step had a duration of 6 min and a current intensity, expressed in terms of C-rate, of 1C, providing a variation of 10% of the initial SOC (see Figure 3).

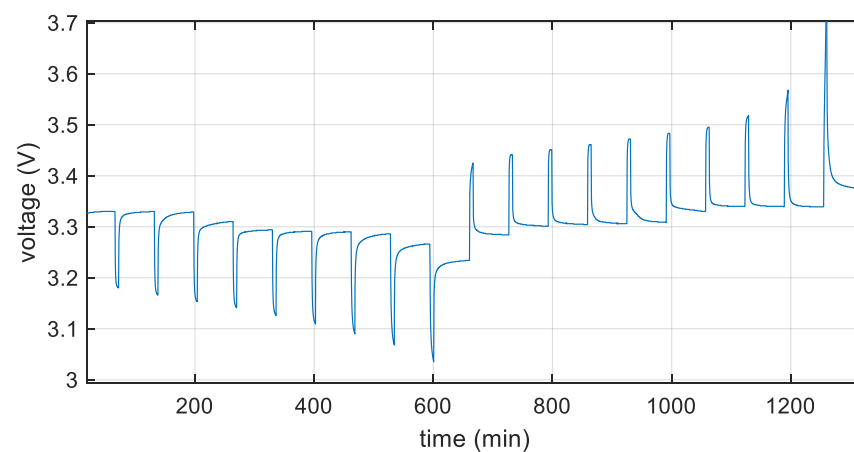


Figure 3. Example of voltage profile during MST.

With the MST, cell parameters were calculated for discrete values of SOC and referring to a fixed value of internal cell temperature. The repetition of the same test at different temperatures expanded the calibration of electrical parameters also in function of cell temperature.

The first parameter that was obtained was the cell V_{OC} by a direct measure of the voltage after one hour of rest. For the interval $10\% \leq SOC \leq 90\%$, a couple of measures were obtained—one during the discharge phase and the other during the charge—so V_{OC} was set as the mean value between the two, while a single value was recorded at $SOC = 100\%$ and $SOC = 0\%$ as well. V_{OC} values in function of SOC and temperature are displayed in Table 2.

Table 2. Cell open circuit voltage.

SOC	V_{OC} (V) at 298.15 K	V_{OC} (V) at 313.15 K	V_{OC} (V) at 328.15 K
0%	3.234	3.226	3.224
10%	3.275	3.270	3.267
20%	3.294	3.293	3.292
30%	3.297	3.300	3.303
40%	3.298	3.302	3.303
50%	3.301	3.303	3.306
60%	3.320	3.314	3.314
70%	3.335	3.335	3.335
80%	3.335	3.335	3.336
90%	3.335	3.336	3.336
100%	3.375	3.434	3.503

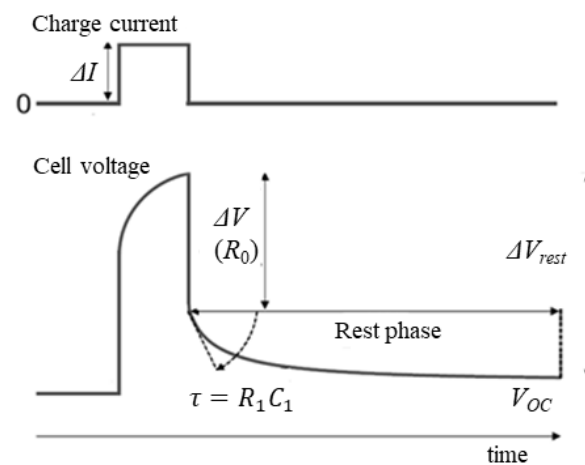
The other electric parameters were calculated as follows, referring to the stylized scheme of Figure 4:

$$R_0 = \Delta V / \Delta I \quad (5)$$

where ΔV and ΔI are respectively the cell instantaneous output voltage difference and output current difference, derived from the MST test, both taken over the one-second interval after the end of a discharge (or charge) step.

$$R_1 = \frac{\Delta V_{rest}}{\Delta I} - R_0 \quad (6)$$

where ΔV_{rest} is the voltage variation during a rest phase and ΔI is the same as before.

**Figure 4.** Example of a generic charge step in an MST test.

The following equations describe the voltage versus time dynamic during the rest phase; the first one (7) after a discharge period, the second one (8) after a charge:

$$V_{cell}(t) = (V_{OC} - V_{rest0})(1 - e^{-\frac{t}{\tau}}) + V_{rest0} \quad (7)$$

$$V_{cell}(t) = (V_{rest0} - V_{OC})(e^{-\frac{t}{\tau}}) + V_{OC} \quad (8)$$

with V_{rest0} the starting voltage of a rest phase and τ the circuit time constant. After calculating the value of τ that best fits the experimental data, the circuit capacitance C_1 is obtained as:

$$C_1 = \tau / R_1 \quad (9)$$

Table 3 reports R_0 , R_1 , and C_1 mean values for each discrete SOC value, as they are obtained during both charge and discharge phases of MST. The columns refer to three

reference temperatures, each one representative of a single MST test. As the calibration interval was set to be $SOC\ 10\% \leq SOC \leq 90\%$ and $298.15\ K \leq T \leq 328.15\ K$, a bivariant (SOC, T) linear interpolation function was used to calculate any missing value located within or outside the calibration interval.

Table 3. Electrical model parameters.

SOC	R_0 (m Ω)			R_1 (m Ω)			C_1 (kF)		
	298.15 K	313.15 K	328.15 K	298.15 K	313.15 K	328.15 K	298.15 K	313.15 K	328.15 K
10%	1.41	1.00	0.83	1.42	1.03	0.79	191.4	148.8	120.1
20%	1.39	0.98	0.83	1.41	1.06	0.81	168.7	210.3	155.0
30%	1.38	0.98	0.83	1.35	1.02	0.82	140.1	138.4	231.6
40%	1.37	0.97	0.84	1.30	1.00	0.79	150.1	116.9	139.3
50%	1.34	0.96	0.82	1.30	0.98	0.79	246.6	163.6	134.2
60%	1.32	0.95	0.81	1.27	1.03	0.81	268.3	496.2	410.5
70%	1.32	0.95	0.82	1.33	1.00	0.79	101.7	121.6	130.3
80%	1.31	0.95	0.82	1.43	1.03	0.80	75.6	84.6	99.1
90%	1.33	0.96	0.81	1.73	1.21	0.92	61.0	74.0	86.3

3.2. Thermal Model and Calibration of Its Parameters

The thermal model shown in Figure 5 is a first order lumped parameters model that can be described through an equivalent electric circuit characterized by a heat source (P_{heat}), a thermal capacity (C_{core}), a conductive thermal resistance (R_{cond}), and a convective thermal resistance (R_{conv}) [20]. T_{core} , T_{surf} , are respectively core and surface temperature of the cell, while T_{amb} is the ambient temperature.

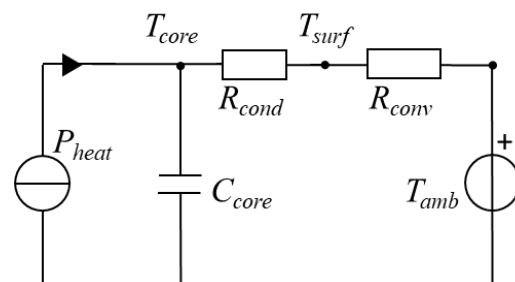


Figure 5. Equivalent electrical circuit for the lithium cell.

The thermal model consents to define cell temperatures via the following equations:

$$C_{core} \frac{dT_{core}}{dt} + \frac{T_{core}(t) - T_{amb}(t)}{R_{cond} + R_{conv}} - P_{heat}(t) = 0 \quad (10)$$

$$P_{heat}(t) = I^2 R_0 + I_1^2 R_1 \quad (11)$$

Battery heat generation is usually defined as the sum of an irreversible term due to the Joule effect and a reversible one due to internal entropic changes [21]. Despite that, in Equation (11), heat generation takes into account only the Joule effect, while the cell entropy variation term is omitted: various studies confirm that for such LFP cells, the reversible heat generation term is negligible if compared with the irreversible one [9,22].

In order to determine the thermal parameters of the cell (C_{core} , R_{cond} , R_{conv}), a thermal characterisation test was followed, as in [9]. During this test, the cell was repeatedly discharged to $SOC = 20\%$ and charged back to $SOC = 80\%$ by a fixed current intensity of 1C. The series of alternating discharge and charge phases produced cell heating, causing internal and surface cell temperatures to progressively rise until a periodic stabilised regime was achieved, in which each temperature only varied in a limited range, defined by local maximum and minimum values.

Figure 6 reports the experimental temperature dynamics of the electrode, of the cell surface, and of the room obtained during the thermal characterisation test. As visible, it is possible to distinguish a first part, in which we have a periodic stabilised regime—e.g., having a temperature oscillation limited within a narrow band—and a last part, when the current is set to zero, in which we observe a thermal relaxation.

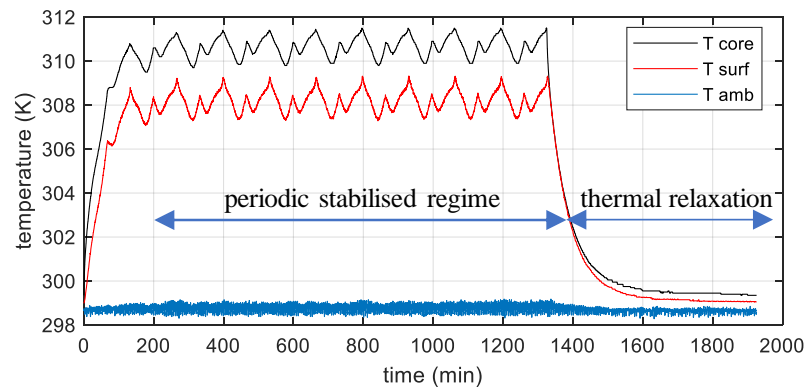


Figure 6. Thermal characterisation test temperature profiles.

Given the impossibility of directly measuring the internal cell temperature, in this test, the latter was assumed as the temperature acquired by the probes located on the cell electrodes due to the high thermal conductivity of the electrode materials, as reported in [9]. Because of that, in Figure 6, experimental electrode temperature is labelled as T_{core} .

However, it is important to underline that the assumption of the electrode temperature equal to the internal cell temperature is valid only for the current profile of this specific thermal characterisation test. Further validation tests, consisting of more intense and variable current profiles, will show that the aforementioned hypothesis is no longer valid for such cases.

Once acquiring the temperature profiles, an estimation of thermal resistances R_{cond} , R_{conv} is obtained as follows:

$$R_{cond} = \frac{T_{core_{SS}} - T_{surf_{SS}}}{\bar{P}_{heat}} \quad (12)$$

$$R_{conv} = \frac{T_{surf_{SS}} - T_{amb_{SS}}}{\bar{P}_{heat}} \quad (13)$$

where $T_{core_{SS}}$, $T_{surf_{SS}}$, and $T_{amb_{SS}}$ are averaged values calculated during the steady-state period, and \bar{P}_{heat} is the average value of cell-generated heat calculated with Equation (11) during the same time span.

Instead, C_{core} is then calculated during the thermal relaxation phase in environmental air (final period of Figure 6). The cell is pre-heated, and no current is flowing. The cell temperature time evolution during the thermal relaxation can be described by the following equation, and shown in the next Figure 7:

$$T_{core}(t) = (T_{core0} - T_{amb_{\infty}}) \cdot e^{-t/\tau_{th}} + T_{amb_{\infty}} \quad (14)$$

where T_{core0} is the initial condition, and $T_{amb_{\infty}}$ is the average air temperature during the thermal relaxation part. The term τ_{th} represents the thermal time constant, and by calculating the value that best fits the experimental data as reported in Figure 7, cell thermal capacity is obtained as:

$$C_{core} = \frac{\tau_{th}}{R_{cond} + R_{conv}} \quad (15)$$

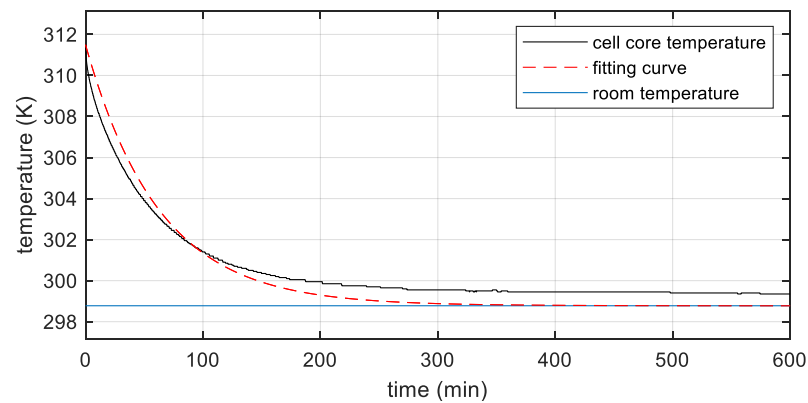


Figure 7. Experimental thermal relaxation for cell thermal capacity estimation. Black curve: cell core temperature. Dashed red curve: the fitting results achieved with Equation (14). Blue curve: room temperature.

The following Table 4 table resumes the obtained results from the cell thermal characterization.

Table 4. Thermal characterisation results.

$T_{core_{ss}}$ (K)	310.65
$T_{surf_{ss}}$ (K)	308.15
$T_{amb_{ss}}$ (K)	298.75
\bar{P}_{heat} (W)	7.56
R_{cond} (K/W)	0.33
R_{conv} (K/W)	1.25
C_{core} (J/K)	2383

4. Electro-Thermal Model Validation

4.1. Test Description

The proposed electro-thermal model was developed in the MATLAB environment and considered in three main validation tests, whose characteristics are shown in Table 5. The tests 1 and 2 are based on typical battery current profiles gained from a numerical simulation model [23] adapted to a BEV (pure battery electric vehicle) running on the Class 3 category of world-wide harmonized light duty driving test cycle (WLTC), indicative of vehicles driven in Europe and Japan [24]. In particular about test 1, after a 1C discharging for a duration of 360 s, the WLTC current profile was imposed and scaled in order to match a maximum discharge current of 3C, as in the upper plot of Figure 8. About test 2, after a 1C discharging for the same duration, the current profile was remodelled to reach a maximum charge current of about 4C, while during discharge, current values exceeding that limit were cut to 250 A (see always Figure 8). Test 2 was meant to be an intensive test for both electric and thermal solicitation in order to validate the model even in case of higher cell temperatures, with respect to test 1. Finally, test 3 instead validated the model against a 1C constant current discharge.

Table 5. List of validation tests.

Test	Current Profile	Peak Current (A)		Room Temperature Set Point (K)	SOC Range (%)
		Discharge	Charge		
1	WLTC	180	−111	298.15	100–59
2	WLTC	250	−250	298.15	100–24
3	Constant discharge	60	0	298.15	100–0

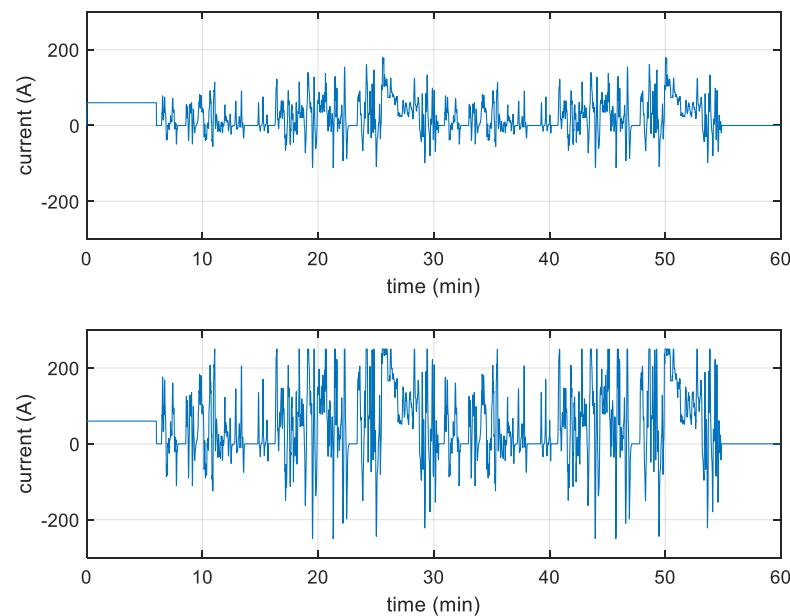


Figure 8. WLTC current profiles. First plot referring to validation test 1, the other referring to test 2. Positive current during discharge.

For every simulated test, the initial conditions of the model were $SOC = 100\%$ (fully charged cell) and model temperatures were set equal to the average value recorded by the respective thermocouples before starting. The other input to the model was the current profile, as imposed in the experimental test.

According to the symbols used in Figure 2, Appendix A shows the plot related to the currents flowing in the R_1C_1 block—e.g., I_1 and I_2 for the reader's convenience, always under test 1 solicitation.

4.2. Simulation Results

The model outputs that were chosen as validation indicators were the cell voltage and surface temperature, as both are the main safety control variables to be monitored. Both cell voltage and surface temperature simulated curves were compared with the respective experimental data as follows:

$$\varepsilon_{V_{cell}}(t) = 100 \cdot \frac{V_{cell_{exp}}(t) - V_{cell_{mod}}(t)}{V_{cell_{exp}}(t)} \quad (16)$$

$$\Delta T_{surf}(t) = T_{surf_{exp}}(t) - T_{surf_{mod}}(t) \quad (17)$$

$\varepsilon_{V_{cell}}$ is cell voltage percentage error, while ΔT_{surf} is the surface temperature deviation. In each formula, the subscript *exp* refers to the experimental measure, acting as the reference value, while the subscript *mod* indicates the model simulation result.

Table 6 reports for all validation tests a series of aggregating factors such as root mean square error (RMSE), mean value, and standard deviation for absolute values of voltage percentage error $\varepsilon_{V_{cell}}$, and the maximum, mean, and standard deviation for the absolute surface temperature deviation ΔT_{surf} .

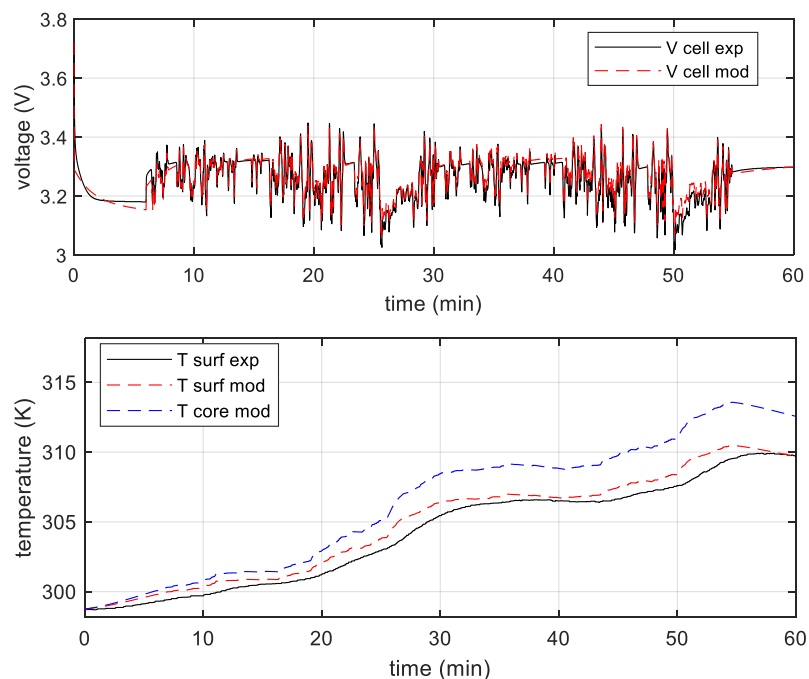
Table 6. Validation tests results.

Test Number	Voltage RMSE (mV)	$ \varepsilon_{V_{cell}} $		$ \Delta T_{surf} $ (K)		
		Mean	Std	Max	Mean	Std
1	21	0.5%	0.4%	0.6	0.2	0.2
2	25	0.6%	0.5%	1.5	0.6	0.3
3	28	0.8%	0.5%	1.1	0.9	0.2

Starting from the contents shown in Table 6, the following main considerations can be remarked. First of all, the model correctly reproduced the experimental voltage profile in all cases and provided reliable results also for the cell surface temperature: in fact, with respect to the actual experimental data, maximum absolute error was lower than 1 K for test 1.

The model also offered a calculation of the core temperature, as it is the temperature at which each set of electric parameters is estimated at every timestep. Despite that, a direct comparison with experimental core temperature was not available, as the approximation of internal cell temperature as the electrode temperature was not proven to be reliable for the performed validation tests reported in Table 6, which largely differ from the ones related to parameter calibration, such as tests reported in Figure 6.

An example of simulation plots regarding experimental and modelled voltage ($V_{cell_{exp}}$, $V_{cell_{mod}}$), experimental and modelled surface temperatures ($T_{surf_{exp}}$, $T_{surf_{mod}}$), and modelled core temperature ($T_{core_{mod}}$) during test 2, are depicted in Figure ??.

**Figure 9.** Experimental data and model simulation for voltage and temperature profiles, test number 2.

An important result relates to the surface temperature estimation: despite an increase of more than 10 K from start to end of the test, the model constantly provided accurate values, with a mean absolute deviation less than 1 K.

In the following, different conditions are analysed in order to assess whether the thermal model calibration assumption, i.e., the core temperature equal to the electrode temperature, can be or cannot be taken as reference also with more significant thermal solicitations.

To accomplish that, the simulation was then repeated for different and much more realistic case studies (e.g., test 1, 2, and 3), forcing the model internal temperature to be equal to the registered temperature at the electrodes. In Table 7, results of voltage errors of this scenario are reported.

Table 7. Model voltage error in case of experimental electrode temperature taken as reference.

Test Number	Voltage RMSE (mV)	$ \varepsilon_{V_{cell}} $	
		Mean	Std
1	22	0.5%	0.5%
2	38	0.8%	0.9%
3	29	0.8%	0.5%

If compared with Table 6, which refers to the estimation of the voltage error as originally evaluated by the model, the results show slightly increasing errors between modelled and experimental voltage, especially for test 2. More interesting results are related to temperature estimation. The illustration in Figure 10 reports both the previously obtained results given by the model with electrical parameters referring to the estimated internal cell temperature ($T_{core_{mod}}$, $T_{surf_{mod}}$), as well as the results achieved by the model with electrical parameters calculated referring to electrode temperature ($T_{core_{exp}}$, $T_{surf_{var}}$). In particular, as assumed, $T_{core_{exp}}$ represents experimental data from ring thermocouples placed on the electrodes, while $T_{surf_{var}}$ is the model surface temperature obtained when electrode temperature is chosen as the indicator of internal temperature, and it is shown by the purple curve.

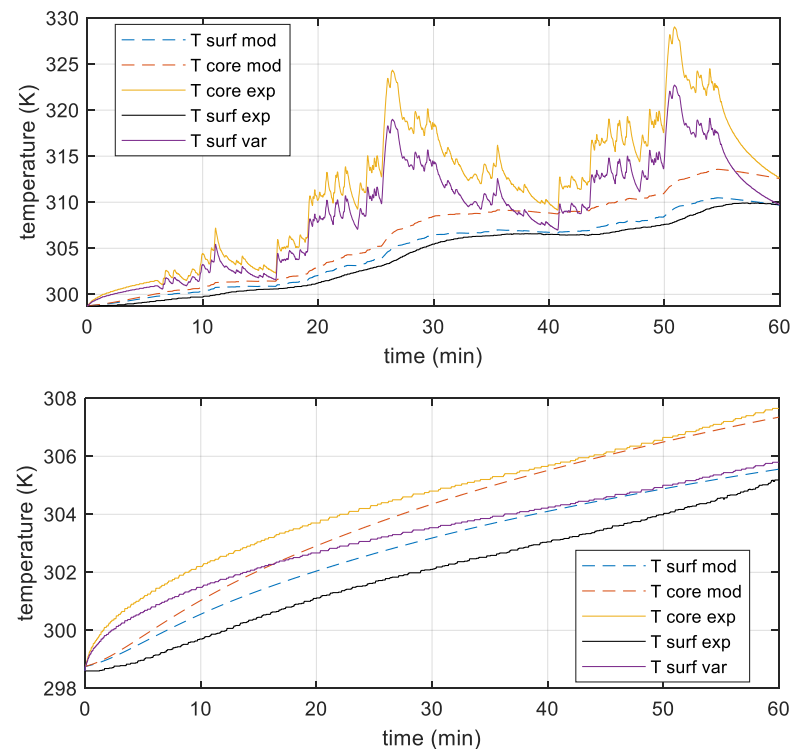


Figure 10. Comparison between experimental data and model simulation: tests number 2 (first plot) and 3 (second plot).

In particular, for test 2, an overestimation of surface temperature with respect to the experimental data from thermocouples $T_{surf_{exp}}$ can be observed, as shown by the purple curve of the upper plot of Figure 10. This means that, when model considers temperature

at the electrodes as the internal reference, and significant current solicitations are modelled (as the ones adopted in test 2), the model does not work properly, especially in representing the core and surface cell temperatures.

Instead, test 3, which involves a current rate limited to 1C, as in the thermal characterization test, shows that electrode experimental temperature $T_{core_{exp}}$ and model internal temperature $T_{core_{mod}}$ are well aligned, as reported in the second plot of Figure 10. In addition, the same accuracy is also observed for the surface temperatures $T_{surf_{mod}}$ and $T_{surf_{var}}$.

These last results confirm that the assumption of considering internal cell temperature equal to the one measured on the cell electrodes appears to be acceptable only for currents in the same range of the one used for the thermal characterisation test (1C). This supports the legitimacy of referring to experimental electrode temperatures for parameter calibration purposes.

5. Conclusions

This paper has shown the development of an electro-thermal model for a LFP lithium cell, able to simulate the cell voltage as well as surface and internal temperature profiles. The model electric parameters were calibrated through specific tests conducted both in discharge and charge, performed at different temperatures. A thermal characterisation test defined thermal parameters. The model parameters were ruled by a two variable interpolation that considered SOC and internal cell temperature and was implemented in a MATLAB simulation environment.

Model outputs were validated by comparison with the experimental cell voltage and surface temperature profiles. All the voltage percentage error between model and measure data never overcame a mean value of 1%, with a maximum absolute temperature error lower than 2 K. Despite the model's simplicity, it also guarantees a correct reproduction of lithium cell behaviour even in the case of working conditions that cause a quick cell temperature rise.

Moreover, the model provides an estimation of the internal cell temperature, underlining the criticality of assuming electrode temperature as an indicator of internal cell conditions, which is allowed only in the case of bland thermal solicitation of the cell, such as for thermal characterisation purposes. Indeed, the problem of measuring the internal cell temperature through probes connected at the electrodes does not appear to be reliable, especially when high current rates are demanded. This may be caused by the local Joule effect heat generation concentrated at the cell terminal connections, which overcomes the cell internal heat generation in the case of high-power demand.

Despite that, a proper validation of core temperature estimation by comparison with a direct measure is still lacking because of the impossibility of safely reaching the centre of the cell without damaging it. An additional limitation is the applicability of the model to a single cell; further tests and improvements will concentrate on the development of the model for also describing a battery pack composed by several cells.

Author Contributions: Conceptualization, M.C. and G.L.; methodology, C.S. and M.B.; validation, C.S.; investigation, M.B.; data curation, C.S.; writing — original draft preparation, M.B.; writing — review and editing, G.L.; visualization, G.L.; supervision, M.C. and G.L. All authors have read and agreed to the published version of the manuscript.

Funding: This research received no external funding.

Institutional Review Board Statement: Not applicable.

Informed Consent Statement: Not applicable.

Conflicts of Interest: The authors declare no conflict of interest.

Appendix A

By taking as reference the circuit already described in Figure 2, plots related to currents I_1 and I_2 versus time under test 1 solicitation are reported in the following Figure A1.

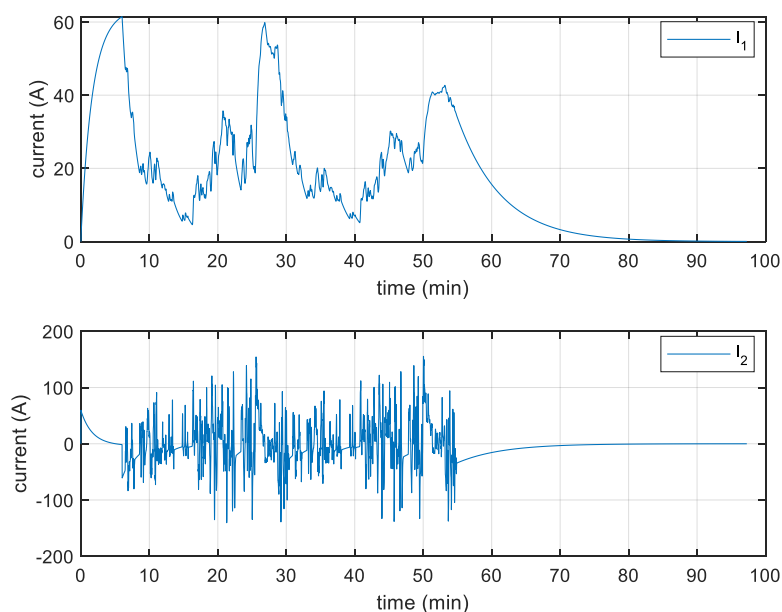


Figure A1. WLTC current I_1 (top) and I_2 (bottom) profiles, test 1 solicitation.

References

1. Wu, W.; Wang, S.; Wu, W.; Chen, K.; Hong, S.; Lai, Y. A critical review of battery thermal performance and liquid based battery thermal management. *Energy Convers. Manag.* **2019**, *182*, 262–281. [CrossRef]
2. Liu, H.; Wei, Z.; He, W.; Zhao, J. Thermal issues about Li-ion batteries and recent progress in battery thermal management systems: A review. *Energy Convers. Manag.* **2017**, *150*, 304–330. [CrossRef]
3. Chang, C. Factors Affecting Capacity Design of Lithium-Ion Stationary Batteries. *Batteries* **2019**, *5*, 58. [CrossRef]
4. Zhang, J.; Zhang, L.; Sun, F.; Wang, Z. An Overview on Thermal Safety Issues of Lithium-ion Batteries for Electric Vehicle Application. *IEEE Access* **2018**, *6*, 23848–23863. [CrossRef]
5. Wang, T.; Li, C.; Chang, L.; Duan, B.; Zhang, C. Thermal behavior analysis of Pouch Lithium ion Battery using distributed electro-thermal model. In Proceedings of the 2019 3rd Conference on Vehicle Control and Intelligence (CVCI), Hefei, China, 21–22 September 2019; pp. 1–5.
6. Wei, P.; Li, H.-X. Two-Dimensional Spatial Construction for Online Modeling of Distributed Parameter Systems. *IEEE Trans. Ind. Electron.* **2022**, *1*. [CrossRef]
7. Kleiner, J.; Komsijska, L.; Elger, G.; Endisch, C. Modelling of 3D Temperature Behavior of Prismatic Lithium-Ion Cell With Focus on Experimental Validation Under Battery Electric Vehicle Conditions. In Proceedings of the 2019 25th International Workshop on Thermal Investigations of ICs and Systems (THERMINIC), Lecco, Italy, 25–27 September 2019; pp. 1–6.
8. Makinejad, K.; Arunachala, R.; Arnold, S.; Ennifar, H.; Zhou, H.; Jossen, A.; Changyun, W. A Lumped Electro-Thermal Model for Li-Ion Cells in Electric Vehicle Application. *World Electr. Veh. J.* **2015**, *7*, 1–13. [CrossRef]
9. German, R.; Shili, S.; Sari, A.; Venet, P.; Bouscayrol, A. Characterization Method for Electrothermal Model of Li-Ion Large Cells. In Proceedings of the 2017 IEEE Vehicle Power and Propulsion Conference (VPPC), Belfort, France, 11–14 December 2017; pp. 1–6.
10. Li, Y.; Du, J.; Lu, L.; Ouyang, M. Analysis on Self-heating Process of Battery Modules in Energy Storage Station Based on Equivalent Circuit Model. In Proceedings of the 2021 IEEE 5th Conference on Energy Internet and Energy System Integration (EI2), Taiyuan, China, 22–24 October 2021; pp. 3894–3899.
11. Damay, N.; Forgez, C.; Bichat, M.-P.; Friedrich, G. Thermal modeling of large prismatic LiFePO₄ / graphite battery. Coupled thermal and heat generation models for characterization and simulation. *J. Power Sources* **2015**, *283*, 37–45. [CrossRef]
12. Guo, Z.; Xu, J.; Xua, Z.; Mubashir, M.; Wang, H.; Mei, X. A Three-Heat-Source Electro-Thermal Coupled Model for Fast Estimation of the Temperature Distribution of a Lithium-ion Battery Cell. *IEEE Trans. Transp. Electrification* **2021**, *8*, 288–297. [CrossRef]
13. Barbieri, M.; Ceraolo, M.; Lutzemberger, G.; Scarpelli, C.; Pessa, T.; Giovannucci, M. Simplified Electro-Thermal Model For Lithium Cells Based On Experimental Tests. In Proceedings of the 2020 AEIT International Conference of Electrical and Electronic Technologies for Automotive (AEIT AUTOMOTIVE), Turin, Italy, 18–20 November 2020; pp. 1–6.
14. Huang, S.; Wu, X.; Cavalheiro, G.M.; Du, X.; Liu, B.; Du, Z.; Zhang, G. In Situ Measurement of Lithium-Ion Cell Internal Temperatures during Extreme Fast Charging. *J. Electrochem. Soc.* **2019**, *166*, A3254–A3259. [CrossRef]
15. Digatron Official Site. Available online: <https://www.digatron.com/en-us/Solutions/Battery-Laboratory> (accessed on 1 April 2022).
16. Binder Official Site. Available online: <https://www.binder-world.com/it> (accessed on 1 April 2022).
17. Mousavi, S.M.; Nikdel, M. Various battery models for various simulation studies and applications. *Renew. Sustain. Energy Rev.* **2014**, *32*, 477–485. [CrossRef]

18. Barsali, S.; Ceraolo, M.; Li, J.; Lutzemberger, G.; Scarpelli, C. Luenberger Observer for Lithium Battery State-of-Charge Estimation. In *ELECTRIMACS 2019*; Zamboni, W., Petrone, G., Eds.; Springer International Publishing: Cham, Switzerland, 2020; Volume 615, pp. 655–667.
19. Ceraolo, M.; Lutzemberger, G.; Poli, D.; Scarpelli, C. Model Parameter Evaluation for Nickel-Manganese-Cobalt Cells: An Examination and Verification of Various Approaches. *IEEE Ind. Appl. Mag.* **2021**, *27*, 29–36. [[CrossRef](#)]
20. Samanta, A.; Williamson, S.S. A Comprehensive Review of Lithium-Ion Cell Temperature Estimation Techniques Applicable to Health-Conscious Fast Charging and Smart Battery Management Systems. *Energies* **2021**, *14*, 5960. [[CrossRef](#)]
21. Bernardi, D.; Pawlikowski, E.; Newman, J. A General Energy Balance for Battery Systems. *J. Electrochem. Soc.* **1985**, *132*, 5–12. [[CrossRef](#)]
22. Panchal, S.; Dincer, I.; Agelin-Chaab, M.; Fraser, R.; Fowler, M. Thermal modeling and validation of temperature distributions in a prismatic lithium-ion battery at different discharge rates and varying boundary conditions. *Appl. Therm. Eng.* **2016**, *96*, 190–199. [[CrossRef](#)]
23. Ceraolo, M.; Lutzemberger, G.; Doveri, N. Experiences of realisation and test of a fuel-cell based vehicle. In Proceedings of the SPEEDAM 2010, Pisa, Italy, 14–16 June 2010.
24. WLTC Site. Available online: <https://dieselnet.com/standards/cycles/wltp.php> (accessed on 1 April 2022).